Talanta 254 (2023) 124113

Contents lists available at ScienceDirect

Talanta

journal homepage: www.elsevier.com/locate/talanta

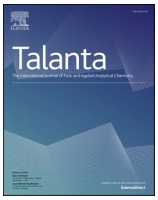

Raman spectroscopy and NIR hyperspectral imaging for in-line estimation of fatty acid features in salmon fillets

Tiril Aurora Lintvedt [a,b,*], Petter Vejle Andersen [a], Nils Kristian Afseth [a], Karsten Heia [a], Stein-Kato Lindberg [a], Jens Petter Wold [a]

[a] Norwegian Institute for Food, Fisheries and Aquaculture Research, Muninbakken 9-13, Breivika, Tromsø, 9291, Norway
[b] Faculty of Science and Technology, Norwegian University of Life Sciences, Ås, 1432, Norway

ARTICLE INFO

Keywords:
Raman Spectroscopy
NIR hyperspectral Imaging
In-line food evaluation
Representative sampling
Salmon quality
Omega-3 fatty acids

ABSTRACT

Raman spectroscopy was compared with near infrared (NIR) hyperspectral imaging for determination of fat composition (%EPA + DHA) in salmon fillets at short exposure times. Fillets were measured in movement for both methods. Salmon were acquired from several different farming locations in Norway with different feeding regimes, representing a realistic variation of salmon in the market. For Raman, we investigated three manual scanning strategies; i) line scan of loin, ii) line scan of belly and iii) sinusoidal scan of belly at exposure times of 2s and 4s. NIR images were acquired while the fillets moved on a conveyor belt at 40 cm/s, which corresponds to an acquisition time of 1s for a 40 cm long fillet. For NIR images, three different regions of interest (ROI) were investigated including the i) whole fillet, ii) belly segment, and iii) loin segment. For both Raman and NIR measurements, we investigated an untrimmed and trimmed version of the fillets, both relevant for industrial in-line evaluation. For the trimmed fillets, a fat rich deposition layer in the belly was removed. The %EPA + DHA models were validated by cross validation (N = 51) and using an independent test set (N = 20) which was acquired in a different season. Both Raman and NIR showed promising results and high performances in the cross validation, with $R2_{CV}$ = 0.96 for Raman at 2s exposure and $R2_{CV}$ = 0.97 for NIR. High performances were obtained also for the test set, but while Raman had low and stable biases for the test set, the biases were high and varied for the NIR measurements. Analysis of variance on the squared test set residuals showed that performance for Raman measurements were significantly higher than NIR at 1% significance level (p = 0.000013) when slope-and-bias errors were not corrected, but not significant when residuals were slope-and-bias corrected (p = 0.28). This indicated that NIR was more sensitive to matrix effects. For Raman, signal-to-noise ratio was the main limitation and there were indications that Raman was close to a critical sample exposure time at the 2s signal accumulation.

1. Introduction

For many years, the health effects of the omega-3 fatty acids eicosapentaenoic acid (EPA) and docosahexaenoic acid (DHA) have gained much attention [1–6]. Fat rich fish, such as Atlantic salmon, is a major source of EPA and DHA in the human diet and therefore, the abundance of these fatty acids can be considered an important quality parameter in the aquaculture industry. Today most of the salmon found in the stores are farmed, and studies have shown that feed is the main factor determining fatty acid composition of the muscle of Atlantic salmon [7–9]. It is also known that other factors such as genetics can influence [10–12]. In later years, there has been a trend to replace marine ingredients in feed with vegetable oils, resulting in lower abundance of EPA and DHA [13–15]. A challenge is that low levels of EPA and DHA have been connected to low fish welfare in sea cages and low fillet quality [16,17]. This emphasizes the motivation to monitor fatty acid features in salmon more closely. Continuous monitoring of EPA and DHA in salmon fillets could provide opportunities for salmon farms to obtain continuous knowledge on impact of different feeding regimes and potentially other farming parameters. It could also provide the opportunity to report specific quality features to consumers, resulting in increased consumer trust and more targeted quality differentiation. Preferably, measurement stations should be integrated on the conveyor belt, scanning each single fillet. For this to be realized, a robust and rapid in-line

* Corresponding author. Norwegian Institute for Food, Fisheries and Aquaculture Research, Muninbakken 9-13, Breivika, Tromsø, 9291, Norway.
E-mail address: tiril.lintvedt@nofima.no (T.A. Lintvedt).

https://doi.org/10.1016/j.talanta.2022.124113
Received 29 June 2022; Received in revised form 14 November 2022; Accepted 16 November 2022
Available online 1 December 2022

measurement technique is needed. Two of the practically relevant methods in this respect are Raman spectroscopy and near infrared spectroscopy (NIRS).

The reported use of NIRS for estimation of omega-3 fatty acids in pure fish oils is promising [18,19]. However, estimation of specific fatty acids in intact salmon fillets is more challenging due to lower concentrations and more interferants, such as water and protein. Brown et al. [20] utilized NIR spectra in the range 800–1850 nm and reported moderate performances for prediction of EPA and DHA in intact salmon cutlets, which indicated compatibility with rough screening applications only. In addition, it was unclear if these models relied on indirect modelling on total fat, as discussed by Eskildsen et al. [21] An advantage of NIRS (400–2500 nm) is that hyperspectral imaging instruments are available and reasonably affordable. NIR hyperspectral imaging has been successfully used for determination of total fat content and fat distribution in whole salmon fillets [22–24]. These instruments already allow very fast measurements of whole fillets on the conveyor belt. In an in-line situation, imaging ensures representative measurements of whole salmon fillets and provides the opportunity for distributional analysis. To the authors knowledge there are no studies concerning EPA and DHA measurements in salmon fillets using NIR hyperspectral imaging which include the spectral region above 1700 nm. This region is likely important for more robust modelling of unsaturated fatty acids since it is associated with the CH═CH vibration [25].

Raman spectroscopy is a promising tool for compositional analysis of fatty acids [26–29]. In a recent work, Lintvedt et al. [30] demonstrated the potential use of in-line Raman spectroscopy for samples of ground salmon which were passing by on the conveyor belt. Here it was shown that the spectra had sufficient quality at high speeds and could be used for estimation of the fatty acids %EPA + DHA. However, fast non-contact Raman measurements of intact salmon fillets have not been investigated, and the challenge that is posed by the heterogeneity of the fillets should be addressed. Raman spectroscopy is practically challenging due to sensitivity to ambient light signals in the production hall, the limited focal volume and the need for timing the signal accumulation. Since the Raman focal volume is small, the collection of representative measurements from a heterogeneous fillet is not self-evident. By using a so called wide area illumination probe one can obtain larger measurement areas (spot size diameter 3–6 mm) than with traditional Raman instrumentation which in addition provides insensitivity to smaller variations in working distance [31]. The latter is important when measuring samples varying in thickness. The signal-to-noise ratio (SNR) is a limiting factor for Raman when exposure time is reduced to only a few seconds [30]. Fat is a relatively strong Raman scatterer, so stronger Raman signals will be obtained on fat rich tissue. The fat deposition in salmon gradually increases from loin to belly and from tail to head, and as much as 49% of the belly flap wet weight can be lipids. This means that it is important to determine the optimal sampling region on the fillets, and for in-line Raman measurements, robotics can be used to implement this critical sampling. This motivates an investigation of different strategies for robotic control of the Raman probe, i. e to determine what is the optimal scanning path.

Although Raman spectroscopy is practically more challenging to employ in the industry, the method could have considerable advantages with respect to robustness of the %EPA + DHA predictions. Firstly, Raman scattering originate from fundamental vibrational transitions yielding a lower degree of overlapping spectral bands (e.g. between protein and fat) compared to NIR spectra [19]. This is because NIR absorptions are based on overtones and combination modes, in contrast [32]. In addition, water signals can dominate NIR spectra, while it is well known that water is a very weak Raman scatterer and is usually not a challenge. Robust methods can potentially reduce the needed frequency of re-calibrations. Although relevant Raman instrumentation is currently about twice the cost of NIR hyperspectral cameras, the potential gain from less effort on model maintenance represents a considerable cost reduction, which should be considered. Afseth et al. [33] compared Raman and NIR laboratory measurements of homogenized salmon samples (N = 668) and found that chemical information on fatty acids in Raman measurements are much better resolved than in NIR measurements. This study also showed that Raman had significantly higher cross validated performances for estimation of EPA and DHA, indicating that Raman might be the more robust solution. However, at higher speeds, signal-to-noise ratio (SNR) can be a limitation for Raman as pointed out above. Therefore it is of interest to compare the two methods in a relevant in-line setup employing short exposure times.

In this work, the main aim was to investigate the feasibility of in-line Raman measurements of %EPA + DHA in single intact salmon fillets employing a wide area Raman probe and to compare the robustness of this method with measurements with an NIR hyperspectral camera (930–2500 nm). The model generalization ability to new samples was mainly demonstrated through predictions on an independent test set. For Raman spectroscopy, in-line measurements were manually mimicked by employing short exposure times of several different scanning paths over the fillet. For the same samples, NIR images were acquired while the fillets moved on a conveyor belt at 40 cm/s, investigating different regions of interest (ROI). For both Raman and NIR measurements, we investigated a fat trimmed and an untrimmed version of the fillets, which are both relevant for industrial in-line evaluation. To the best of our knowledge, this is the first time the feasibility for in-line Raman measurements of %EPA + DHA prediction in intact salmon fillets is investigated and compared with NIR hyperspectral imaging (930–2500 nm).

2. Material and methods

2.1. Salmon fillets

A calibration set of 51 salmon fillets was acquired from five different farming locations with varying feeding regimes from three different Norwegian suppliers (SalMar ASA, Norway Royal Salmon ASA and Lerøy Seafood Group ASA). Salmon were supplied as whole gutted fish stored on ice in which state they were kept for about 5 days in a cold room at 1–2 °C before filleting. Subsequently the right fillet was vacuum packed and frozen (−30 °C) and used for the NIR measurements which were carried out in a different location. The left fillet was immediately used for the Raman measurements. Thawing of the salmon fillets before the NIR experiment was done on racks in a room with air circulation for about 2 h, then they were kept in a cold room (1–2 °C) over night. Approximately half a year later, an independent test set consisting of 20 salmon fillets was acquired from three different farming suppliers with different feeding regimes. The test set was treated the same way as the calibration set.

Two fillet versions were measured in both Raman and NIR experiments. First, each fillet was measured untrimmed, with a surface layer of deposited fat and bones covering the muscle fibers in the belly. Afterwards, the surface layer of deposited fat and bones were trimmed away while keeping as much intact belly muscle as possible. Fillets were stored in a cold room at 1–2 °C during the experiment time.

2.2. Measurements and data analysis

2.2.1. Raman measurements

We employed a MarqMetrix All-in-One (AIO) Raman system covering a Raman shift range of 100–3250 cm^{-1}. The system was equipped with a 785 nm laser operating at 450 mW power and the sampling optic was a wide area illumination (D = 3 mm), Proximal BallProbe HV standoff Raman probe (MarqMetrix Inc., Seattle, WA, USA) with working distance at approximately 9 cm. Each salmon fillet was placed on a PE plastic plate covered with aluminium foil. The foil was used to prevent potentially disturbing signals from the plate plastic. We mimicked in-line scans manually in a dark room, with the help of a movable instrument rack for the probe. One person pushed the fillet

forward while another handled the rack which allowed the probe to be moved transversely to the speed direction, resulting in the three different scanning strategies illustrated in Fig. 1 and denoted as S1) line scan of loin, S2) sinusoidal scan of belly and S3) line scan of belly. The result was one accumulated spectrum for each of the illustrated paths. The different scans were chosen to elucidate the effect of varying fat deposition across the salmon fillet on spectra and performance. Two different accumulation times were applied: 4s and 2s, where 4s represented fast at-line measurements and 2s was regarded short enough to be relevant in the process line. Three replicate measurements were acquired for each combination of scanning path and accumulation time.

2.2.2. NIR measurements

We employed a hyperspectral camera (HySpex SWIR-384) from Norsk Elektro Optikk (NEO) with spectral range 930–2500 nm that employs an MCT detector cooled down to 150 K. Diffuse halogen lighting was used for illumination, and measurements were done in reflectance mode. The fillets moved on a conveyor belt at a speed of 40 cm/s, which correspond to an acquisition time of 1s for a 40 cm long fillet. The images were collected from a working distance of approximately 1 m with an acquisition speed of 200 frames per second. The focus plane was about 4 cm over the conveyor belt. For the 51 calibration fillets, one image scan was collected per fillet. For the test set fillets, 3 replicate measurements were acquired.

2.2.3. Reference measurements

Since the right fillet was frozen and sent to a different location for NIR imaging, the reference samples were prepared from the belly of the trimmed left-side fillets as indicated in Fig. 2b. The variation between the left and right fillet was assumed to be negligible. The bellies were homogenized (Retsch Knife Mill GRINDOMIX GM 200, 7000 rpm for 3s), vacuum packed and frozen at −30 °C. Analyses of the samples were carried out by BioLab (Bergen, Norway). Fatty acid concentrations were determined by gas chromatography (capillary GC-FID) on fatty acid methyl esters (AOCS Official Method Ce 1b-89), and were expressed as a percentage of the total fat in the analyzed sample. The total fat of the belly samples was determined by the Bligh and Dyer method [34].

2.2.4. Estimation of iodine value

As a measure of total unsaturation in the salmon, the iodine value (IV) was estimated from the full fatty acids (FA) profile in accordance with the AOCS recommended practice Cd 1c-85, and same as reported by Berhe et al. [35] and Afseth et al. [33].

$$IV = M_w(I_2)\sum_{i=1}^{n}\frac{DB_{(i)}V_{FAMe(i)}}{M_w(FAMe_{(i)})} \quad (1)$$

where M_w is molecular weight, I_2 is iodine, $FAMe(i)$ is the fatty acid methyl ester number i, DB is the number of double bonds and $V_{FAMe(i)}$ is percentage of fatty acid number i.

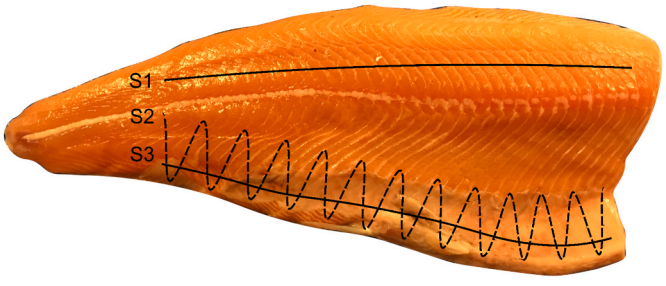

Fig. 1. Scanning strategies for Raman signal accumulation, including S1) line scan of loin, S2) sinusoidal scan of belly, and S3) line scan of belly.

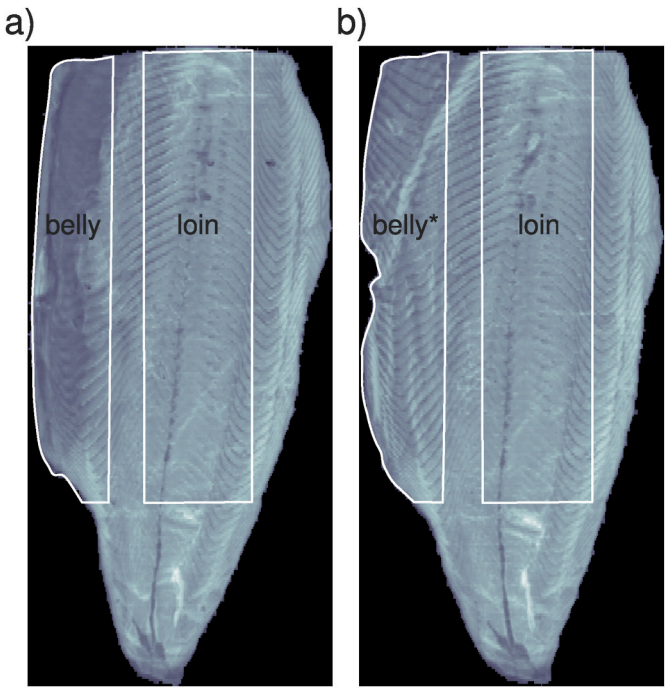

Fig. 2. Example of hyperspectral NIR images (1210 nm shown) for one salmon fillet in untrimmed (a) and trimmed (b) version, with the belly and loin ROIs indicated by the white outlines. References were prepared from the corresponding belly area (*) of the fillet used for the Raman experiment.

2.2.5. Pre-processing of spectral data

For Raman spectra, the Raman shift range 520–1800 cm^{-1} was used in analyses. Cosmic ray spikes were removed manually by a simple spike detection algorithm based on derivatives. Subsequently Savitsky-Golay (SG) smoothing (polynomial order 2 and window size 9) [36] was applied, followed by Extended Multiplicative Signal Correction (EMSC) [37,38] employing up to the sixth order polynomial and the Asymmetric Least Squares (ALS) algorithm [39,40] for baseline correction of the EMSC reference spectrum. The ALS reference spectrum correction employed a smoothing parameter of 5.8 and an asymmetric weighting parameter (of the residuals) of 0.01. For the test set spectra, pre-processing by EMSC employed the mean spectrum of the calibration samples as the reference spectrum. Pre-processing was applied separately on subsets which were defined by the combinations of fillet version, scanning paths and exposure time.

The NIR hyperspectral images were radiance calibrated in the Hyspex Rad V2.5 software (NEO, Oslo, Norway) and reflectance values were calculated through division by a spectralon white reference. Each reflectance spectrum was then transformed to the pseudo-absorbance ($A = \log_e(1/R)$). An average spectrum across all pixels was used for further analysis. For each image, three different regions of interest (ROI) were investigated, where we used the i) whole fillet, ii) belly region and iii) loin region, as indicated in Fig. 2. The average spectra were pre-processed by regular EMSC employing linear and quadratic polynomials for baseline correction and the spectral region 1170–1850 nm was selected and used for further analysis to avoid the noisy region above 2000 nm. Similar to the Raman spectra, pre-processing on NIR spectra was applied on the separate subsets which were defined by the combinations of fillet version and ROIs. Between the two periods of acquisition of calibration data and test set data, the camera was repaired and a small wavelength shift occurred. This required an additional wavelength interpolation for the test set sample spectra.

2.2.6. Data modelling

Partial least squares regression (PLSR) [41,42] was used for

calibration development. We established models for EPA + DHA concentration in salmon fillets. Note that EPA and DHA concentrations were not estimated separately, but as a joint concentration value. PLSR models were built on the 51 calibration fillets. For selection of optimal number of latent variables for the models, we employed cross-validation (CV), where replicate measurements were held out in the same CV segment to avoid overfitting. The reason for not averaging the replicates was to keep the prediction conditions as close to an in-line situation as possible. The choice of number of latent variables for the PLS modelling was based on a simple criterion using a 3% punish factor, as described by Westad and Martens [43]. The model was then rebuilt on the full calibration set with the optimum number of components and applied on the pre-processed test set spectra. We report performance through the coefficient of determination (R2) and the root mean squared error (RMSE). For the test set validation, we also report these metrics when corrected for slope and bias errors, together with the bias and slope. To establish whether the estimation errors of the test set using Raman spectra were significantly different from those using NIR hyperspectral images, we applied a two-way analysis of variance (ANOVA) of the squared residuals. In addition, the confidence intervals of the coefficient of determination (R2) were reported in some figures. These were calculated from the Fisher Z-transformation [44,45].

2.3. Signal to noise ratio

In this work, we compared the SNR of sets of spectra obtained by different Raman measurement strategies. First, the spectra in the given set were pre-processed as described in section 2.2.5. Then, the SNR of each spectrum was calculated as the ratio between the average spectrum and the standard deviation of the estimated noise, according to Eq. (2). The reported value for one set was the average SNR of all individual spectra in the respective set.

$$SNR = \frac{mean(I)}{sd(I_n)} \tag{2}$$

where I is the spectrum intensity and I_n is the estimated noise intensity. The noise component of the spectrum was estimated by subtracting a smoothed version of the spectrum from the original spectrum I. This resulted in a residual spectrum I_n containing mainly noise. For smoothing we used SG with polynomial order 2 and window size 9. This is similar to Guo et al. [46] and same as in our previous work [30].

2.3.1. Repeatability of predictions

For the test set, 3 replicates were acquired for both Raman and NIR. The repeatability of the measurements by each method was calculated as the pooled standard deviation of the predictions within the replicate groups

$$STD_{pooled} = \sqrt{\sum_{j=1}^{M}\sum_{i=1}^{N}\frac{(\hat{y}_{ij} - \overline{Y}_j)}{M(N-1))}} \tag{3}$$

where M is the number of salmon fillets, N is the number of replicate measurements and $\hat{y}_{ij}$ is the predicted value of replicate number i in replicate group number j. The average prediction within the replicate group number j is denoted by $\overline{Y}_j$.

3. Results and discussion

3.1. Sample variation in fat composition

The calibration samples spanned a range of %EPA + DHA levels (4.6–10.5%) and DHA/EPA ratios (1.1–2.4) representing typical effects of different feeds. The test set samples spanned a similar %EPA + DHA range (4.5–12.3%), but had a less even distribution due to the lower number of samples. Moreover, there was a shorter span in DHA/EPA ratio (1.1–1.6) and higher overall fat level than in the calibration samples. The higher fat level in the test set corresponded well with expected seasonal variations in fat deposition. Note also that the test set represented some extrapolation in %EPA + DHA levels in comparison to the calibration set. See supplementary for distributions in FA properties (Fig.A.7).

3.2. Spectral features

The Raman spectra (Fig. 3a) were dominated by bands associated with fatty acids. The main absorption bands related to fatty acid unsaturation are the C=C stretch (1657 cm^{-1}) and the alkene C–H bend (1266 cm^{-1}) [27,28]. The peak around 930 cm^{-1} is most likely related to the alkene C–H deformation in polyunsaturated fatty acid moieties [47,48]. The main bands related to fatty acid saturation are the methylene scissor deformation (1440 cm^{-1}) and the methylene twisting deformation (1302 cm^{-1}). Other bands of interest originate from the aromatic ring breathing of phenylalanine (1004 cm^{-1}) and the liquid aliphatic C–C stretch in gauche (1080 cm^{-1}) [27,28].

The NIR spectra (Fig. 3b) had broader bands which overlapped and a baseline related to e.g. scattering effects was apparent. The main absorption bands are associated with the second overtone of the CH stretch (1210 nm [49]), the CH stretch first overtone (1723, 1761 nm [25,50]) and OH stretch first overtone (1400 nm [49]). The shoulder around 1164 nm is related to the degree of unsaturation and is an important peak for estimation of iodine value [25,51]. Furthermore, the CH band at 1761 nm has been primarily related to saturated fatty acids, while literature indicate that a shift of the band around 1723 nm towards shorter wavelengths is related to the degree of unsaturation [25,49]. The spectral region above 2000 nm was noisy and detrimental for model performance, and therefore discarded from the further analyses. It should be noted that some bands of interest are located in this region [49,50].

3.3. Implication of Raman sampling strategies

Regression results from employing the different Raman sampling methods, i.e. different fillet versions and scan paths, are shown in Table 1. Differences in Raman signal level as a consequence of the different sampling strategies were clearly visible in the spectra (Fig. 3), and were reflected in the SNR levels (Table 1). Scans of typical high fat regions had higher intensity, with highest signals from measurements of the untrimmed belly, followed by the scans of the trimmed belly. The sinusoidal belly scans had slightly lower signals compared to the corresponding line scans. The loin scans exhibited considerably weaker signals. From the cross validation on the designated calibration set, it was evident that the loin scan stood out with the poorest model errors ($R2_{CV} = 0.77$ at 4s exposure and $R2_{CV} = 0.56$ at 2s exposure) as well. All belly scan variations gave high performances at both 4s and 2s exposure. Part of the reason for the low performances from loin measurements can also be that the reference sample was taken from belly, and moderate variations in FA composition across the fillet is possible [52]. However, in previous work [30], we found that %EPA + DHA estimation based on Raman spectra was limited by the SNR level. Together, these results indicate that pointing the Raman probe toward areas with high fat deposition is important to acquire spectra with sufficient quality at short exposure times.

Measurements on untrimmed fillets gave the overall highest performances across the two exposure times. While the fillet trimming did not seem to greatly affect the estimations at 4s exposure, there was a moderate impact at 2s, with lower $R2_{CV}$ (Table 1). The impact of scan path was less discernible. The differences seen between the measurement strategies are at least partly connected to the SNR. The $R2_{CV}$ correlated closely with SNR at 2s exposure ($r_{2s} = 0.99$), but not at 4s exposure ($r_{4s} = 0.67$). This indicated that the signal strength gained from measuring on the untrimmed fillets and from choosing the optimal scan

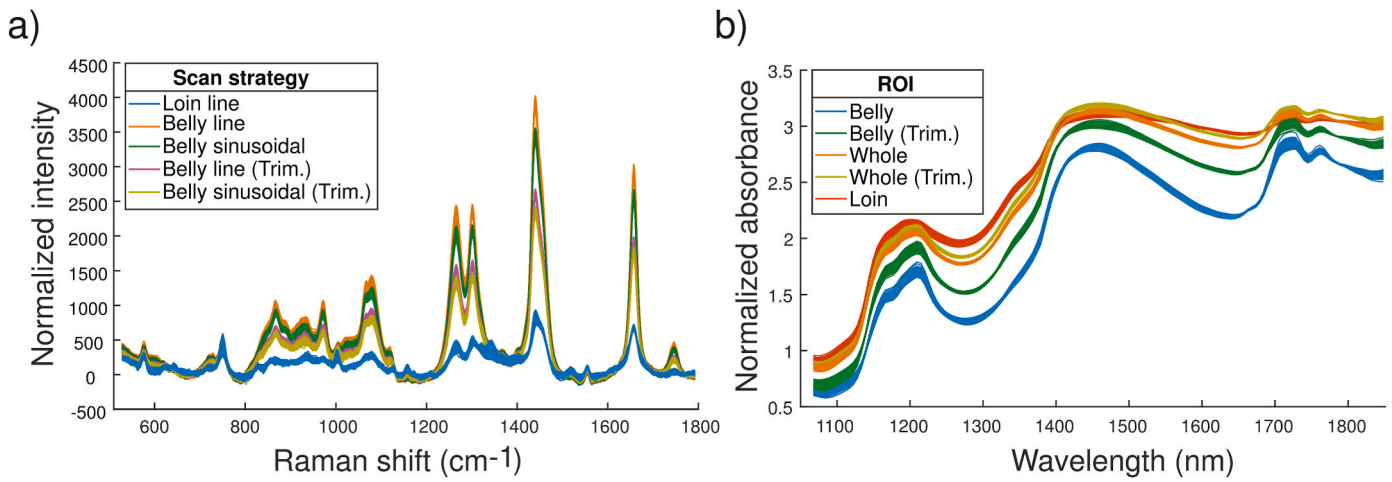

Fig. 3. Calibration sample spectra from Raman (a) and NIR (b) measurements compared across the respective investigated subset versions, i.e. combinations of exposure time, scanning paths and fillet versions for Raman spectra and combinations of ROIs and fillet versions for NIR spectra. The Raman spectra shown are the 2s exposure time measurements.

Table 1
PLS regression results for EPA + DHA in salmon fillets (% of total fat), using Raman spectra. Cross validated results for the calibration set (CV) and test set validation results are shown. For the test set validation, metrics corrected for bias and slope errors are indicated as well (corr).

Sampling method			Calibration set				Test set					Corrected test set	
Exp.	Fillet version	Scan	LV[a]	$R2_{CV}$	$RMSE_{CV}$	SNR[b]	R2	RMSEP	Bias	Slope	STD_{pooled}[c]	$R2_{corr}$	$RMSE_{corr}$
4s	–	S1	3	0.77	0.77	41.2	–	–	–	–	–	–	–
4s	untrimmed	S2	3	0.95	0.34	66.8	0.94	0.66	−0.14	1.20	0.20	0.99	0.31
4s	untrimmed	S3	3	0.96	0.33	68.0	0.95	0.60	−0.21	1.17	0.14	0.99	0.29
4s	trimmed	S2	3	0.95	0.36	60.8	0.91	0.79	−0.44	1.18	0.23	0.98	0.37
4s	trimmed	S3	3	0.95	0.36	63.0	0.95	0.60	−0.29	1.11	0.25	0.98	0.38
2s	–	S1	2	0.56	1.05	32.2	–	–	–	–	–	–	–
2s	untrimmed	S2	2	0.95	0.35	58.5	0.87	0.98	−0.33	1.31	0.18	0.99	0.29
2s	untrimmed	S3	3	0.96	0.33	60.5	0.96	0.52	−0.24	1.11	0.18	0.99	0.32
2s	trimmed	S2	1	0.91	0.47	51.0	0.93	0.71	−0.35	1.14	0.40	0.98	0.41
2s	trimmed	S3	3	0.93	0.42	53.6	0.88	0.95	−0.54	1.24	0.27	0.98	0.36

[a] Latent variables.
[b] Signal to noise ratio for calibration set.
[c] Pooled standard deviation (repeatability).

path is more important when the scan speed is increased further. Correspondingly, it might indicate that at 2s signal accumulation, we are approaching a critical limit for spectrum quality, while at 4s signal accumulation the Raman scanning approach will likely be more robust towards lower fat levels in fillets. One should bear in mind that there are more information about pigments and other bulk properties in scans of trimmed fillets (e.g. peaks at 1004, 1158, 1342 and 1519 cm^{-1}). See Fig B.9 for easier distinction of Raman peaks between the different measurement strategies. If an in-line system should be coupled with other analyses, it is a greater chance of accomplishing this with trimmed fillets.

With respect to exposure time, we overall saw more uniform results with respect to $R2_{CV}$ and the number of latent variables included in the models at 4s exposure. However, the performances seen at 2s exposure time was very encouraging, as they were considerably improved compared to what was obtained for homogenized salmon samples in previous work [30]. Notably, the SNR in this work was overall comparable to 10s exposure time in the previous work, most likely because the fat content of the measured regions were higher in the current work.

3.4. Implication of sampling strategies for NIR hyperspectral imaging

For NIR spectral data, it was evident (Fig. 3) that spectra from the belly region, particularly for the untrimmed fillets, had less prominent baselines than the spectra from regions which included the loin. This was seen also in the test set data (Fig.B.8b). The differences in baselines were most likely a combination of different tissue structures, which can lead to differences in scattering effects, and that high fat areas are dominated by fat absorbance. This consequently allows less absorption by other interferants such as water, which has broader absorption peaks. Additionally, measurements of the belly and whole untrimmed fillets had relatively stronger fat signals than the measurements of loin and the whole trimmed fillets. Cross validation on the calibration set showed that the effect was that measurements of the separate loin region had considerably lower performance than the measurements from other regions, similar as for Raman. Differences in $R2_{CV}$ between the rest of the ROIs were small, but $R2_{CV}$ increased with fat level of the regions, with measurements of untrimmed belly yielding highest performance. SNR was naturally not the reason (above 2000), and it might rather be because the higher fat signals decreased the relative disturbance from interferants.

3.5. Regression models

EPA (20:5 n-3) and DHA (22:6 n-3) have 5 and 6 double bonds, respectively, and are among the FAs with highest unsaturation. In addition they have long carbon chains. Prediction models are expected to emphasize spectral features related to these characteristics. Typical

Raman regression coefficients (Fig. 4) showed that the main positively correlated peaks were at 926, 1261 and 1666 cm^{-1}, which can all be associated with unsaturated modes, as discussed in section 3.2. The main negatively correlated peaks were at 1012, 1084 and 1442 cm^{-1}, which indicated that there were some indirect modelling of proteins and saturated fatty acids. These are the same characteristics as in previous work on %EPA + DHA estimation in homogenized salmon samples [30,33]. For the NIR models, the positions around 1701–1706 nm and 1160 nm stood out with high positive weights. The positive weighting around 1701–1706 nm in combination with the negative weighting at 1723 suggested that a shift in the peak around 1723 towards lower wavelengths was important for the model. These characteristics are in accordance with high unsaturation [25,49].

3.6. Raman versus NIR hyperspectral imaging

3.6.1. Performance and robustness

The feasibility of in-line estimation of %EPA + DHA using Raman and NIR spectroscopy, as well as the robustness of the established models, were indicated by the cross validation on the calibration set and the test set performances. These results are summarized in Tables 1 and 2. We show also test set performances when predictions are corrected for bias-and-slope errors. Such errors are oftentimes acceptable for deployment in the industry because models can be recalibrated when new sample types are introduced. However, in certain applications (e.g. genetics studies), performance on new samples should be high without the need of a recalibration. Therefore both uncorrected and corrected test set metrics are relevant to consider. Based on the cross validation on the calibration set, results were excellent for both NIR and Raman. This showed that both methods are viable options for estimation of fatty acid features in salmon fillets at high speeds and indicate that both can handle variations in total fat levels and variations in the ratio between EPA and DHA. Overall, the Raman models needed considerably lower numbers of latent variables than the NIR models to reach similar performances. This is in accordance with observations by Afseth et al. [33]

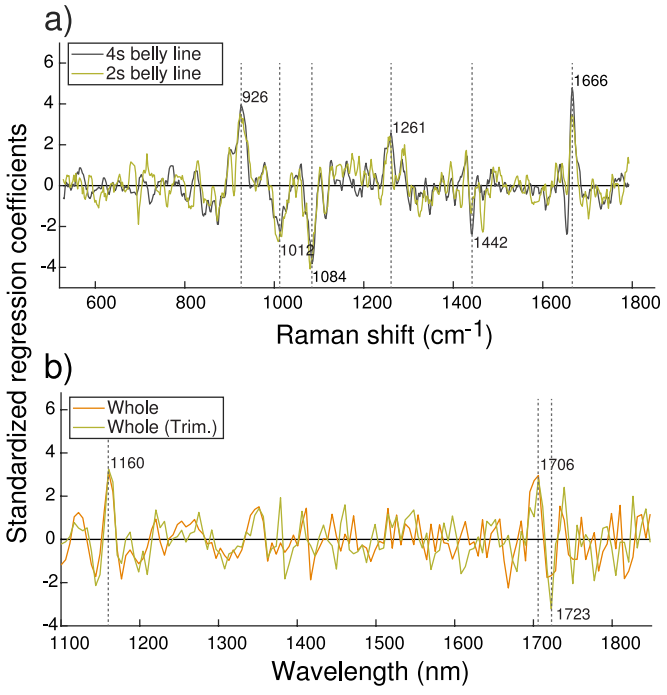

Fig. 4. Standardized regression vectors for the different subsets of Raman data (a) and NIR data (b), as calculated from the calibration set and applied on the test set measurements. For Raman, regression coefficients are shown for both 4s and 2s exposure measurements.

for homogenized salmon and, as they discuss, can be regarded a testimony of the chemical specificity of the Raman spectral features. This makes models more interpretable and might make models less sensitive to interferants. Examples of relevant interferants were signals from water, bone, blood remnants or protein content in fillets, which have more overlapping signals in NIR than for Raman, due to their different nature.

The question was how sensitive these models were to interferants and how dependent they were on conserved correlations between FA parameters in the salmon fillets. This was elucidated by the test set. Predictions on test set samples were generally much less biased for Raman models than the NIR models for which biases were several times higher and varied considerably between different sampling strategies. There was a certain trend (Table 2) that measurements of low fat regions (i.e loin and trimmed fillets) had high biases, while the measurements of high fat regions had lower biases (i.e untrimmed fillets), again reinforcing the impression that higher fat signals decreased the relative spectrum disturbances. The large biases led to odd R2 and RMSEP values. In comparison, biases for the Raman predictions were low and stable for all sampling strategies. In addition, the repeatability of predictions from NIR were overall lower than for Raman, which was reflected by the higher pooled standard deviation of the predictions. For Raman, the repeatability among the different sampling strategies correlated clearly with SNR, and more clearly at 2s exposure time than at 4s ($r_{4s} = -0.83$ and $r_{2s} = -0.94$), which again emphasized the importance of SNR for Raman.

From the bias-and-slope corrected test set predictions, variance errors were identifiable. For both methods, corrected performances were overall excellent. This showed that as long as we assume that slope and bias errors can be corrected during model deployment, NIR is a good option as well. Considering both corrected and uncorrected performances, the best case NIR results were obtained from measurements on untrimmed whole fillets, which stood out with high $R2_{corr}$ values, low bias and the highest repeatability (Table 2). For Raman, the best case result was obtained for line scan on the untrimmed belly, which gave high $R2_{corr}$ values, high repeatability and lowest bias and slope errors (Table 1). For comparison between methods, the Raman measurements at 2s exposure time is most relevant due to the most similar scanning speed as the NIR measuremements. In Fig. 5 we compared the best case test set validation results for NIR and Raman at 2s exposure time. For NIR, R2corr was high for all number of components above 5, but it was evident that some PLS components in the NIR model were particularly disturbing with respect to bias, indicating a more unstable situation than for Raman. In comparison, Raman had high $R2_{corr}$ levels and low bias which were both stable across all components. In addition, there were higher variance errors in the NIR predictions, particularly at low %EPA + DHA levels. This reinforces the importance of high FA signals for NIR. Analysis of variance on the squared test set residuals showed that the best case performance for Raman measurements were significantly higher than NIR at 1% significance level ($p = 0.000013$) when slope-and-bias errors were not corrected, but not significant when residuals were slope-and-bias corrected ($p = 0.28$).

One should keep in mind that, for NIR measurements, differences in water loss due to small deviations in the calibration and test set thawing procedure or differences in sample temperatures might have occurred and influenced results. The repair and recalibration of the NIR instrument between the calibration and test set acquisition could also have an impact. Therefore, any clear conclusion on the comparability of Raman and NIR with respect to robustness of fast in-line %EPA + DHA estimation can not be made. However, this study indicated, in accordance with the nature of the narrow Raman bands versus the broader NIR bands, that Raman is more robust.

3.6.2. Prediction of other fatty acid features

For a broader comparison of the Raman and NIR measurement methods, Fig. C.10 shows predictions of many other FA parameters for

Table 2
PLS regression results for EPA + DHA in salmon fillets (% of total fat), using NIR hyperspectral images. Cross validated results for the calibration set (CV) and test set validation results are shown. For the test set validation, metrics corrected for bias and slope errors are indicated as well (corr).

Sampling method		Calibration set			Test set					Corrected test set	
Fillet version	Region of interest	LV[a]	$R2_{CV}$	$RMSE_{CV}$	R2	RMSEP	Bias	Slope	STD_{pooled}[b]	$R2_{corr}$	$RMSE_{corr}$
–	Loin	13	0.87	0.58	−19.80	12.26	12.19	1.00	0.70	0.80	1.20
untrimmed	Whole	14	0.95	0.37	0.90	0.86	−0.22	1.21	0.19	0.97	0.49
untrimmed	Belly	14	0.97	0.28	−0.08	2.80	−2.72	1.12	0.40	0.97	0.47
trimmed	Whole	16	0.94	0.40	−8.27	8.19	8.15	1.03	0.50	0.93	0.73
trimmed	Belly	15	0.96	0.32	−4.36	6.23	−6.18	1.12	0.51	0.95	0.61

[a] Latent variables.
[b] Pooled standard deviation (repeatability).

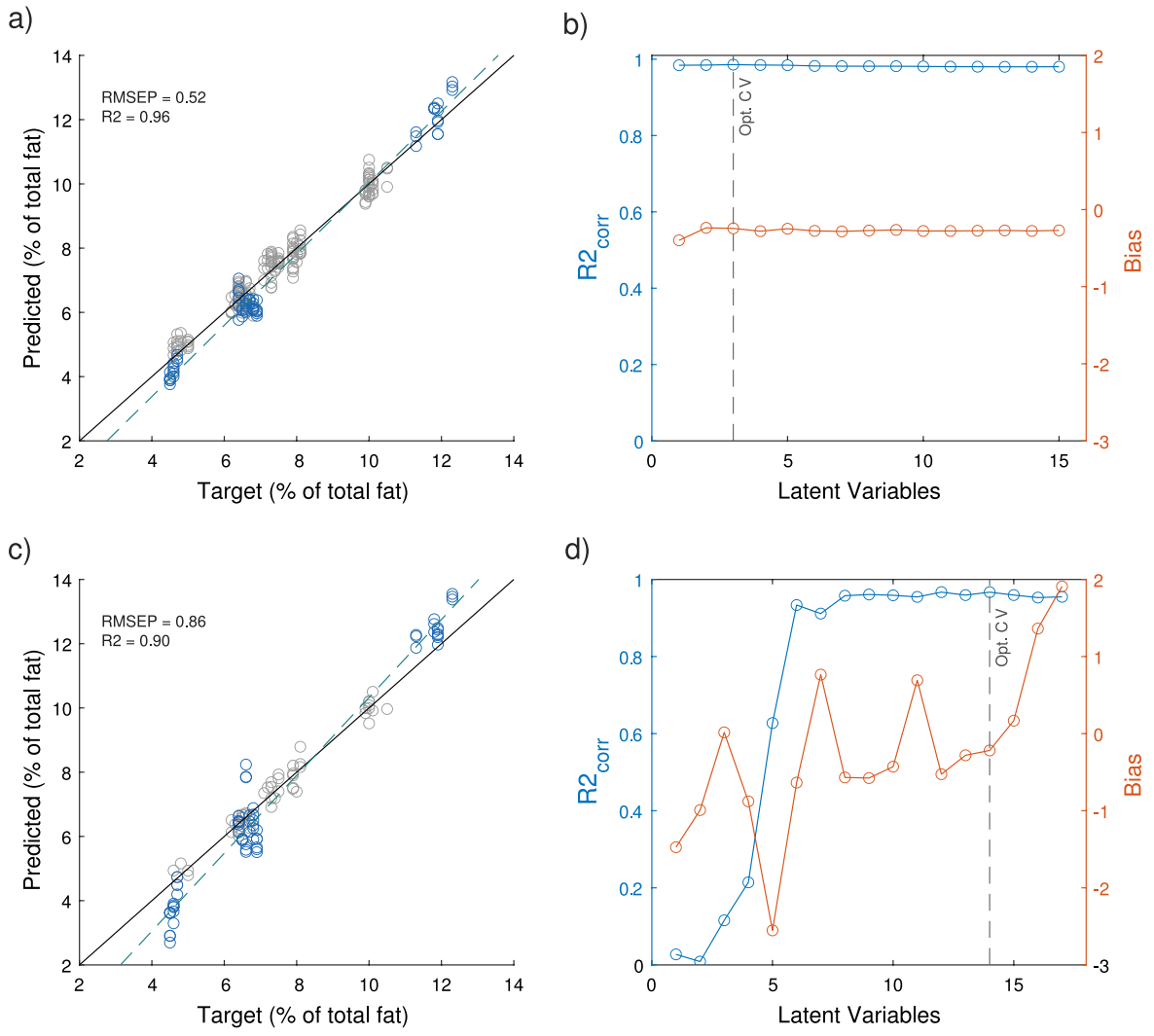

Fig. 5. Overview of the best case results from PLS regression for prediction of %EPA + DHA from Raman measurements at 2*s* exposure time (a–b) and NIR measurements (c–d). The highest Raman performance was obtained from belly line scans of untrimmed fillet. For NIR, highest performance was obtained for the whole untrimmed fillet. The predicted versus measured EPA + DHA concentrations (a,c) for the test set (blue) is included, and compared with the calibration set (grey). The performances on the test set as a function of latent variables in the models are shown (b,d), including bias and R2 corrected for the bias-and-slope errors. (For interpretation of the references to colour in this figure legend, the reader is referred to the Web version of this article.)

the calibration set. Interpretation of the additional models was out of scope for this article, but it should be noted that predictions for most FAs were high. Covariance between EPA + DHA and other fatty acids or chemical components in the salmon fillets can be an issue if the correlations are different in future samples. In literature, model dependence on conserved correlations has been termed the cage of covariance, and challenges related to this issue for estimation of specific FAs have been demonstrated by Eskildsen et al. and others [21,33,35]. In our calibration samples, the strongest correlations with %EPA + DHA were found for the sum of saturated FAs (r = 0.92), sum of monoenoic FAs (r = −0.91) and the fatty acid 18:3 n-3 (r = −0.94). The correlation with total fat in the samples was low (- 0.17). Furthermore, the correlation between EPA and DHA was moderate (r = 0.74), which showed that they to some extent vary independently across different feeding regimes (Fig.

A.6). In the test set samples, the correlations between the FA properties were overall considerably higher than in the calibration samples (Fig. A.6). Predictions on the calibration set (Fig.C.10) showed that separate DHA models were also excellent for both Raman and NIR, but separate EPA models were less successful (albeit not significantly). However, taking into account the high spectral similarity between these two fatty acids [33] and the moderate correlation between them in the calibration set, we cannot expect them to be predicted independently. Predicting the EPA and DHA as a joint concentration value is a good compromise, keeping also in mind that both have been related to positive health effects.

Berhe et al. [35] found that estimation of specific fatty acids in pork backfat from Raman spectra were indirect and to a large degree dependent on the total FA parameters (i.e Iodine value and total PUFA). In our case, the cross validated IV model and total PUFA model showed poor performances for both Raman and NIR (Fig. C.10), which makes it unlikely that %EPA + DHA was indirectly modelled based on total unsaturation (number of double bonds) or total PUFA content. This corresponds to results recently shown by Afseth et al. [33] for homogenized salmon and illustrates that such issues are dependent on the samples and the variations in the calibration set. It can, however, be noted that the salmon in the work of Afseth et al. [33] were all from the same population and were fed a specific diet, and hence represented a sample set with variations of different origin than the sample set used in our work. Interestingly, slope-and-bias-corrected performances on our test set showed that prediction of IV and total PUFA was considerably improved in comparison to the calibration set (Fig. C.11). This is most likely related to the higher correlations with the individual FAs in the test set samples (Fig.A.6). This suggests that IV and PUFA models were based on correlations with specific FAs. In this work, we successfully removed the issue of indirect modelling on total fat content by a combination of estimating the %EPA + DHA content as percentage of total fat, by the sampling method and by normalising spectra by the EMSC pre-processing. This can be seen by the abysmal cross validated performance of total fat estimation for both Raman and NIR (Fig. C.10). The strategy of estimating the %EPA + DHA content as percentage of total fat was also followed by Berhe et al. [35].

Indirect modelling on other chemical components might be an issue as well. There were few samples within each farming location (i.e feed group) and therefore low variance within each group. This increases the risk that models might rely on other dissimilarities between the groups, such as different fillet structures, composition or water content. Band regions related to proteins were weighted negatively in Raman regression coefficients (i.e. phenylalanine), which might suggest that such indirect modelling on protein content come in to play. For Raman, this region can be removed. For NIR, overlapping bands make such solutions harder to find.

3.6.3. Other practical considerations

Choosing Raman or NIR relies also on practical considerations. The scope of possible applications might be different for the two methods. For example, one is often interested in the total fat content in the fillet and not only the composition of the fat. Estimation of total fat content is undoubtedly possible with NIR [22,23] and have already been implemented in the industry. Raman has been used to measure total fat content previously and showed reasonable laboratory results for heterogeneous salmon by-products [53]. However, it could be more challenging with the indicated Raman scanning procedures in this study, since the whole salmon fillet is not covered and heterogeneity is a challenge. Therefore, a system combining total fat analyses with compositional analyses might be harder to achieve with Raman.

Another practical challenge is sample variations over time. During the seasons, the balance between phospholipids and triglycerides (TAGs) of the fillets can vary due to variation in total fat content, with autumn being the main period for fat deposition and spring the main period for fat burning [54–57]. While the phospholipids are quite stable and high in EPA + DHA composition, the composition of the TAGs are to a large extent dependent on the feed [11,58]. Therefore seasonal variations in the total fat level can still affect the FA composition. This means that fatty fillets may have lower EPA + DHA percentage than lean fillets, when measured as % of total fats, while the quantitative EPA + DHA levels could in fact be higher [59]. This should be taken into account in future strategy developments.

With respect to the practical measurements, the SNR was important for Raman. SNR variations across the different subsets correlated considerably with the corresponding estimation errors, suggesting that SNR is the main motivator in choice of measurement strategy. The results indicated that at high conveyor belt speeds, low fat deposition regions of the fillet (i.e the loin) should be avoided during signal accumulation in order to optimize SNR. In practice, this could be achieved by employing robotic control of the probe to target high fat regions of the fillet (i.e the belly). This presents further system development and additional cost for Raman employment in the industry. Furthermore, it is important to investigate the heterogeneity of the salmon fillets more thoroughly. While we know that total fat levels vary over the fillet [52], uncertainty still remains about how much the composition of the fat vary within a fillet. In the study of Nanton et al. [52] examples (N = 3) of moderate differences in EPA and DHA composition in different parts of salmon fillets were seen. Such spatial variations could potentially challenge the Raman measurements. To the author's knowledge, larger studies on compositional variations over a fillet is lacking in the literature and should be conducted.

4. Conclusion

This work showed that a Raman scanning strategy and NIR hyperspectral imaging are both viable methods for in-line measurements of EPA + DHA concentrations in intact salmon fillets. This study indicated that Raman might be more robust towards matrix effects, which likely means a reduced need for calibration maintenance in comparison to NIR. For Raman, the loin scans exhibited too low SNR and resulted in poor performances. Therefore a robotic solution for Raman measurements in the industry might be needed in order to target high fat areas on the fillet during signal accumulation. In addition, there were indications that reducing the exposure time below 2s might be challenging with respect to spectrum quality. This suggested that at this point in time, Raman might be best suited for fast at-line measurements in applications where robustness is important. NIR hyperspectral imaging is currently best suited for industrial employment, but must likely be followed up more closely with calibration maintenance.

Funding

This work was partially funded by the Research Council of Norway through the projects SFI Digital Food Quality and the Food Pilot Plant [grant numbers 309259, 296,083]; along with The Agricultural and Food Industry Research Funds through the project Precision Food Production [grant number 314111].

Credit author statement

Tiril Aurora Lintvedt: Methodology, Formal analysis, Investigation, Data curation, Writing – Original Draft, Visualization. **Petter Vejle Andersen**: Methodology, Investigation, Writing – Review and Editing. **Nils Kristian Afseth**: Conceptualization, Methodology, Writing – Review and Editing, Supervision. **Karsten Heia**: Methodology, Investigation, Writing – Review and Editing, Supervision. **Stein-Kato Lindberg**: Formal Analysis, Investigation. **Jens Petter Wold:** Conceptualization, Methodology, Writing – Review and Editing, Supervision.

Declaration of competing interest

The authors declare the following financial interests/personal relationships which may be considered as potential competing interests: Tiril Aurora Lintvedt reports equipment, drugs, or supplies was provided by MarqMetrix Inc.

Data availability

Data will be made available on request.

Acknowledgements

We would like to express a special thanks to MarqMetrix Inc. for providing Raman instrumentation through the partnership in the SFI Digital Food Quality project. We also extend our thanks to Thomas Larsson, Arnaud Lefrancois, Tatiana N. Ageeva, Amanda Katrine Karlsen, Samuel Ortega Sarmiento, Gustav Martinsen and Ambjørn Bardal at Nofima for assistance during sample preparation and data acquisition.

Appendix A. Correlations and variation in reference measurements

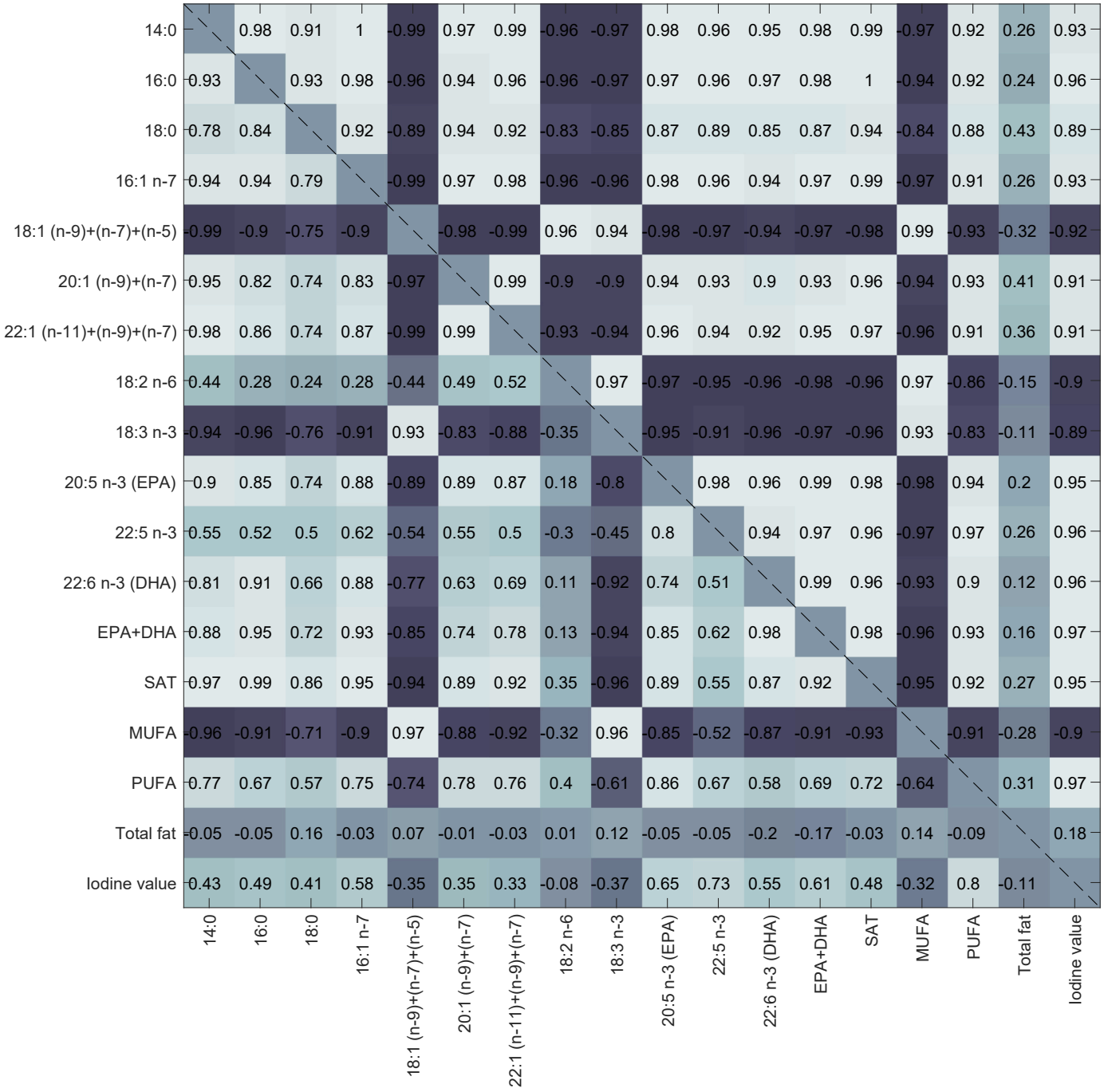

Fig. A.6. Correlation map between reference measurements of the main FAs and total FA parameters for the calibration samples (below diagonal) and the test set samples (above diagonal).

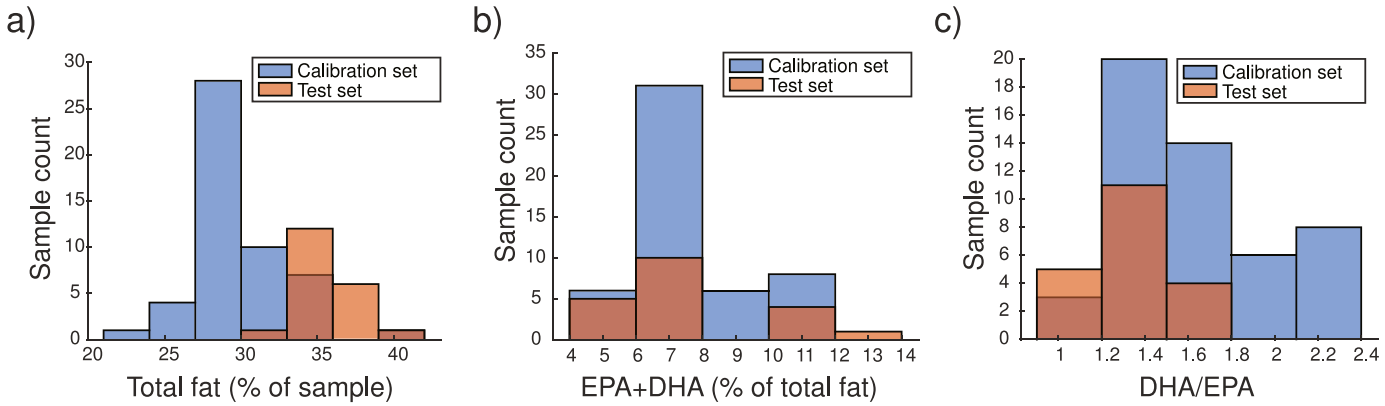

Fig. A.7. Sample distributions of total fat (a), %EPA + DHA (b) and the DHA/EPA ratio, compared between calibration and test set.

Appendix B. Additional spectral data

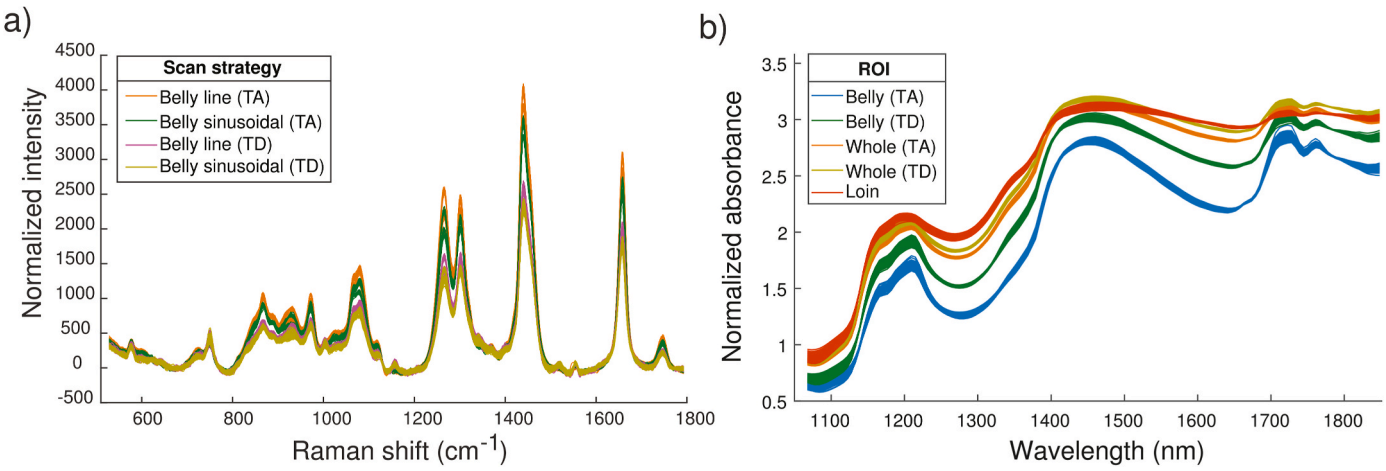

Fig. B.8. Pre-processed Raman test set data (a) and NIR test set data (b).

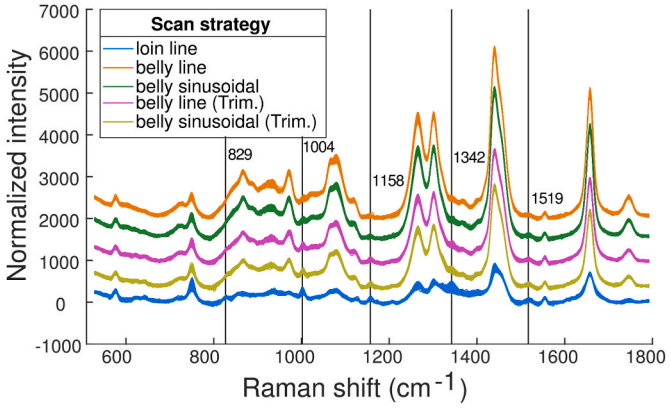

Fig. B.9. Raman measurements of calibration set samples, with introduced offset for clarity.

Appendix C. Modelling additional fatty acid parameters

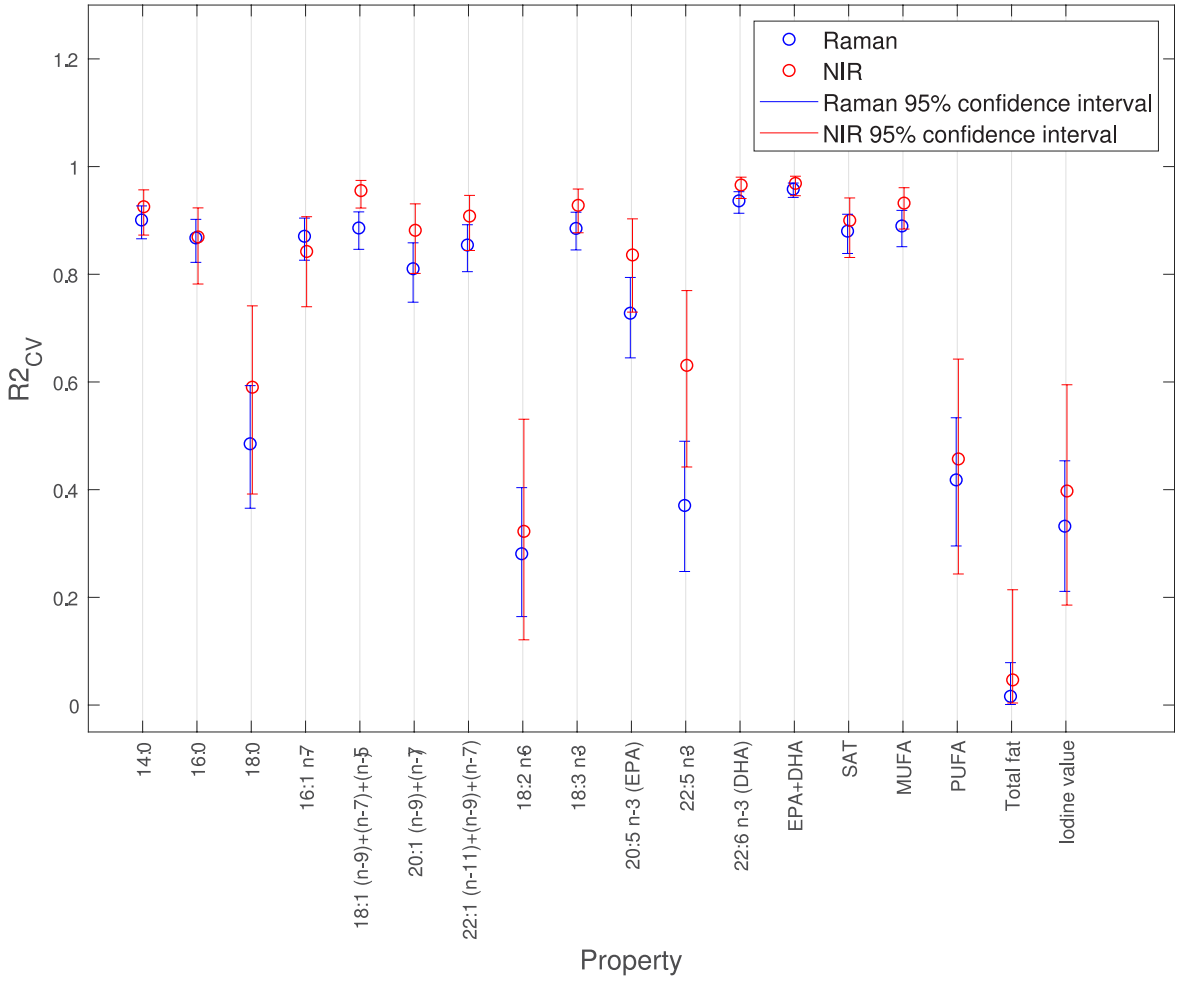

Fig. C.10. Cross validated performances on calibration set for the most important fatty acids parameters, comparing the Raman belly line scans of untrimmed fillet at 2s exposure with the NIR measurements on whole untrimmed fillets. These measurement methods were considered the best case results with respect to %EPA + DHA estimation.

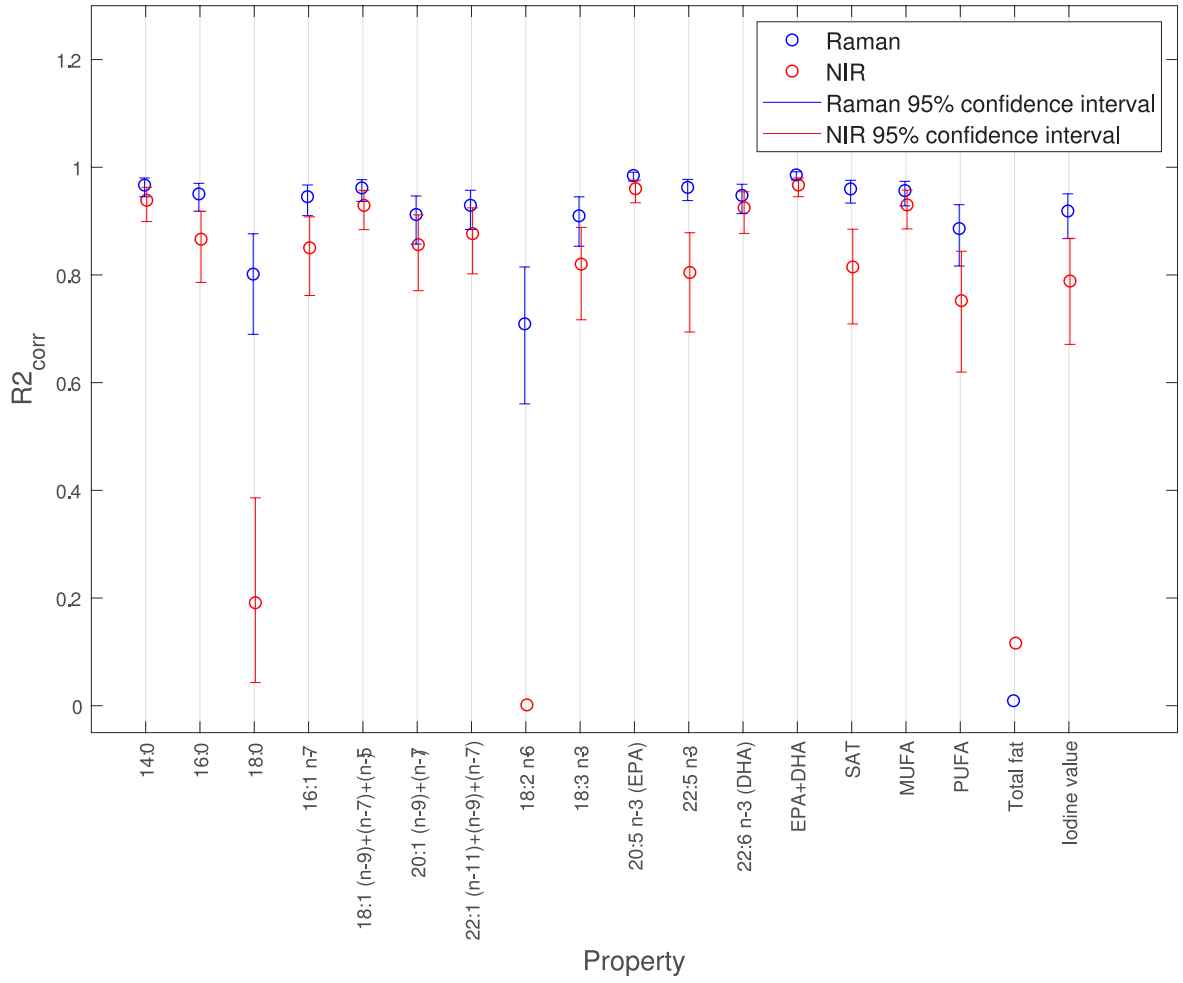

Fig. C.11. Test set performances for estimation of the most important fatty acids parameters, comparing the Raman belly line scans of untrimmed fillet at 2s exposure with the NIR measurements on whole untrimmed fillets. These measurement methods were considered the best case results with respect to %EPA + DHA estimation.

References

[1] P.C. Calder, Marine omega-3 fatty acids and inflammatory processes: effects, mechanisms and clinical relevance, Biochim. Biophys. Acta Mol. Cell Biol. Lipids 1851 (4) (2015) 469–484, https://doi.org/10.1016/j.bbalip.2014.08.010.

[2] A. Eilander, D.C. Hundscheid, S.J. Osendarp, C. Transler, P.L. Zock, Effects of n-3 long chain polyunsaturated fatty acid supplementation on visual and cognitive development throughout childhood: a review of human studies, Prostaglandins Leukot. Essent. Fatty Acids 76 (4) (2007) 189–203, https://doi.org/10.1016/j.plefa.2007.01.003.

[3] M.M. Rogero, P.C. Calder, Obesity, inflammation, toll-like receptor 4 and fatty acids, Nutrients 10 (4) (2018), https://doi.org/10.3390/nu10040432.

[4] C.H. Ruxton, S.C. Reed, M.J. Simpson, K.J. Millington, The Health Benefits of Omega-3 Polyunsaturated Fatty Acids: A Review of the Evidence, oct 2004, https://doi.org/10.1111/j.1365-277X.2004.00552.x.

[5] R.N. Thota, J.J.A. Ferguson, K.A. Abbott, C.B. Dias, M.L. Garg, Science behind the cardio-metabolic benefits of omega-3 polyunsaturated fatty acids: biochemical effects vs. clinical outcomes, Nutrients 9 (7) (2018) 3576–3596, https://doi.org/10.1039/c8fo00348c.

[6] M. Todorčevič, L. Hodson, The effect of marine derived n-3 fatty acids on adipose tissue metabolism and function, J. Clin. Med. 5 (1) (2015), https://doi.org/10.3390/jcm5010003.

[7] J.G. Bell, J. McEvoy, D.R. Tocher, F. McGhee, P.J. Campbell, J.R. Sargent, Replacement of fish oil with rapeseed oil in diets of atlantic salmon (salmo salar) affects tissue lipid compositions and hepatocyte fatty acid metabolism, J. Nutr. 131 (5) (2001) 1535–1543, https://doi.org/10.1093/jn/131.5.1535.

[8] J.G. Bell, J. Pratoomyot, F. Strachan, R.J. Henderson, R. Fontanillas, A. Hebard, D. R. Guy, D. Hunter, D.R. Tocher, Growth, flesh adiposity and fatty acid composition of atlantic salmon (salmo salar) families with contrasting flesh adiposity: effects of replacement of dietary fish oil with vegetable oils, Aquaculture 306 (1–4) (2010) 225–232, https://doi.org/10.1016/j.aquaculture.2010.05.021.

[9] B.E. Torstensen, J.G. Bell, G. Rosenlund, R.J. Henderson, I.E. Graff, D.R. Tocher, Ø. Lie, J.R. Sargent, Tailoring of atlantic salmon (salmo salar l.) flesh lipid composition and sensory quality by replacing fish oil with a vegetable oil blend, J. Agric. Food Chem. 53 (26) (2005) 10166–10178, https://doi.org/10.1021/jf051308i.

[10] S.S. Horn, B. Ruyter, T.H.E. Meuwissen, B. Hillestad, A.K. Sonesson, Genetic effects of fatty acid composition in muscle of atlantic salmon, Genet. Sel. Evol. 50 (1) (2018), https://doi.org/10.1186/s12711-018-0394-x.

[11] D.R. Tocher, J.G. Bell, F. McGhee, J.R. Dick, J. Fonseca-Madrigal, Effects of dietary lipid level and vegetable oil on fatty acid metabolism in atlantic salmon (salmo salar l.) over the whole production cycle, Fish Physiol. Biochem. 29 (3) (2003) 193–209, https://doi.org/10.1023/B:FISH.0000045722.44186.ee.

[12] G.M. Turchini, D.S. Francis, R.S.J. Keast, A.J. Sinclair, Transforming salmonid aquaculture from a consumer to a producer of long chain omega-3 fatty acids, Food Chem. 124 (2) (2011) 609–614, https://doi.org/10.1016/j.foodchem.2010.06.083.

[13] T. Ytrestøyl, T.S. Aas, T. Åsgård, Utilisation of feed resources in production of atlantic salmon (salmo salar) in Norway, Aquaculture 448 (2015) 365–374, https://doi.org/10.1016/j.aquaculture.2015.06.023.

[14] P.D. Nichols, B. Glencross, J.R. Petrie, S.P. Singh, Readily available sources of long-chain omega-3 oils: is farmed australian seafood a better source of the good oil than wild-caught seafood? Nutrients 6 (3) (2014) 1063–1079, https://doi.org/10.3390/nu6031063.

[15] M. Sprague, J.R. Dick, D.R. Tocher, Impact of sustainable feeds on omega-3 long-chain fatty acid levels in farmed atlantic salmon, 2006-2015, Sci. Rep. 6 (2016), https://doi.org/10.1038/srep21892.

[16] M. Bou, G.M. Berge, G. Baeverfjord, T. Sigholt, T.K. Østbye, B. Ruyter, Low levels of very-long-chain n-3 pufa in atlantic salmon (salmo salar) diet reduce fish robustness under challenging conditions in sea cages, J. Nutr. Sci. 6 (2017), https://doi.org/10.1017/jns.2017.28.

[17] E. Lutfi, G. M. Berge, G. Bæverfjord, T. Sigholt, M. Bou, T. Larsson, T. Mørkøre, Ø. Evensen, N. H. Sissener, G. Rosenlund, L. Sveen, T.-K. Østbye, B. Ruyter, Increasing

dietary levels of the n-3 long-chain pufa, epa and dha, improves the growth, welfare, robustness and fillet quality of atlantic salmon in sea cages, Br. J. Nutr. 1–19.
[18] M.M. Cascant, C. Breil, A.S. Fabiano-Tixier, F. Chemat, S. Garrigues, M. de la Guardia, Determination of fatty acids and lipid classes in salmon oil by near infrared spectroscopy, Food Chem. 239 (2018) 865–871, https://doi.org/10.1016/j.foodchem.2017.06.158.
[19] M.Y. Bekhit, B. Grung, S.A. Mjøs, Determination of omega-3 fatty acids in fish oil supplements using vibrational spectroscopy and chemometric methods, Appl. Spectrosc. 68 (10) (2014) 1190–1200, https://doi.org/10.1366/13-07210.
[20] M.R. Brown, P.D. Kube, R.S. Taylor, N.G. Elliott, Rapid compositional analysis of atlantic salmon (salmo salar) using visible-near infrared reflectance spectroscopy, Aquacult. Res. 45 (5) (2014) 798–811, https://doi.org/10.1111/are.12021.
[21] C.E. Eskildsen, T. Næs, P.B. Skou, L.E. Solberg, K.R. Dankel, S.A. Basmoen, J. P. Wold, S.S. Horn, B. Hillestad, N.A. Poulsen, M. Christensen, T. Pieper, N. K. Afseth, S.B. Engelsen, Cage of covariance in calibration modeling: regressing multiple and strongly correlated response variables onto a low rank subspace of explanatory variables, Chemometr. Intell. Lab. Syst. 213 (2021), https://doi.org/10.1016/j.chemolab.2021.104311.
[22] T. Isaksson, G. Tøgersen, A. Iversen, K.I. Hildrum, Non-destructive determination of fat, moisture and protein in salmon fillets by use of near-infrared diffuse spectroscopy, J. Sci. Food Agric. 69 (1) (1995) 95–100, https://doi.org/10.1002/jsfa.2740690115.
[23] J.P. Wold, M. Kermit, V.H. Segtnan, Chemical imaging of heterogeneous muscle foods using near-infrared hyperspectral imaging in transmission mode, Appl. Spectrosc. 70 (6) (2016) 953–961, https://doi.org/10.1177/0003702816641260.
[24] V.H. Segtnan, M. Høy, F. Lundby, B. Narum, J.P. Wold, Fat distribution analysis in salmon fillets using non-contact near infrared interactance imaging: a sampling and calibration strategy, J. Near Infrared Spectrosc. 17 (5) (2009) 247–253, https://doi.org/10.1255/jnirs.851.
[25] F. Westad, A. Schmidt, M. Kermit, Incorporating chemical band-assignment in near infrared spectroscopy regression models, J. Near Infrared Spectrosc. 16 (3) (2008) 265–273, https://doi.org/10.1255/jnirs.786.
[26] N.K. Afseth, V.H. Segtnan, B.J. Marquardt, J.P. Wold, Raman and near-infrared spectroscopy for quantification of fat composition in a complex food model system, Appl. Spectrosc. 59 (11) (2005) 1324–1332, https://doi.org/10.1366/000370205774783304.
[27] N.K. Afseth, J.P. Wold, V.H. Segtnan, The potential of Raman spectroscopy for characterisation of the fatty acid unsaturation of salmon, Anal. Chim. Acta 572 (1) (2006) 85–92, https://doi.org/10.1016/j.aca.2006.05.013.
[28] J.R. Beattie, S.E. Bell, C. Borgaard, A. Fearon, B.W. Moss, Prediction of adipose tissue composition using Raman spectroscopy: average properties and individual fatty acids, Lipids 41 (3) (2006) 287–294, https://doi.org/10.1007/s11745-006-5099-1.
[29] D.P. Killeen, S.N. Marshall, E.J. Burgess, K.C. Gordon, N.B. Perry, Raman spectroscopy of fish oil capsules: polyunsaturated fatty acid quantitation plus detection of ethyl esters and oxidation, J. Agric. Food Chem. 65 (17) (2017) 3551–3558, https://doi.org/10.1021/acs.jafc.7b00099.
[30] T.A. Lintvedt, P.V. Andersen, N.K. Afseth, B. Marquardt, L. Gidskehaug, J.P. Wold, Feasibility of in-line Raman spectroscopy for quality assessment in food industry - how fast can we go? Appl. Spectrosc. 76 (5) (2022) 559–568, https://doi.org/10.1177/00037028211056931.
[31] H. Wikström, I.R. Lewis, L.S. Taylor, Comparison of sampling techniques for in-line monitoring using Raman spectroscopy, Appl. Spectrosc. 59 (7) (2005) 934–941, https://doi.org/10.1366/0003702054411553.
[32] Y. Ozaki, C.W. Huck, K.B. Beć, Near-ir spectroscopy and its applications, in: V. Gupta (Ed.), Molecular and Laser Spectroscopy: Advances and Applications, Elsevier, 2018, pp. 11–38, https://doi.org/10.1016/B978-0-12-849883-5.00002-4. Ch. 2.
[33] N.K. Afseth, K. Dankel, P.V. Andersen, G.F. Difford, S.S. Horn, A. Sonesson, B. Hillestad, J.P. Wold, E. Tengstrand, Raman and near infrared spectroscopy for quantification of fatty acids in muscle tissue—a salmon case study, Foods 11 (962) (2022), https://doi.org/10.3390/foods11070962.
[34] E.G. Bligh, W.J. Dyer, A rapid method of total lipid extraction and purification, Can. J. Biochem. Physiol. 37 (8) (1959) 911–917, https://doi.org/10.1139/o59-099.
[35] D.T. Berhe, C.E. Eskildsen, R. Lametsch, M.S. Hviid, F. van den Berg, S.B. Engelsen, Prediction of total fatty acid parameters and individual fatty acids in pork backfat using Raman spectroscopy and chemometrics: understanding the cage of covariance between highly correlated fat parameters, Meat Sci. 111 (2016) 18–26, https://doi.org/10.1016/j.meatsci.2015.08.009.
[36] A. Savitzky, M.J. Golay, Smoothing and differentiation of data by simplified least squares procedures, Anal. Chem. 36 (8) (1964) 1627–1639, https://doi.org/10.1021/ac60214a047.
[37] H. Martens, E. Stark, Extended multiplicative signal correction and spectral interference subtraction: new preprocessing methods for near infrared spectroscopy, J. Pharm. Biomed. Anal. 9 (8) (1991) 625–635, https://doi.org/10.1016/0731-7085(91)80188-F.
[38] K.H. Liland, A. Kohler, N.K. Afseth, Model-based pre-processing in Raman spectroscopy of biological samples, J. Raman Spectrosc. 47 (6) (2016) 643–650, https://doi.org/10.1002/jrs.4886.
[39] P.H.C. Eilers, H.F.M. Boelens, Baseline correction with asymmetric least squares smoothing, Life Sci. (2005) 1–26.
[40] K.H. Liland, T. Almøy, B.H. Mevik, Optimal choice of baseline correction for multivariate calibration of spectra, Appl. Spectrosc. 64 (9) (2010) 1007–1016, https://doi.org/10.1366/000370210792434350.
[41] H. Martens, T. Næs, Multivariate Calibration, second ed., Wiley, Chichester, UK, 1989.
[42] Å. Björck, U.G. Indahl, Fast and stable partial least squares modelling: a benchmark study with theoretical comments, J. Chemom. 31 (8) (2017), https://doi.org/10.1002/cem.2898.
[43] F. Westad, H. Martens, Variable selection in near infrared spectroscopy based on significance testing in partial least squares regression, J. Near Infrared Spectrosc. 8 (2) (2000) 117–124, https://doi.org/10.1255/jnirs.271.
[44] R.A. Fisher, Frequency distribution of the values of the correlation coefficient in samples from an indefinitely large population, Biometrika (1915), https://doi.org/10.2307/2331838.
[45] R.A. Fisher, On the" probable error" of a coefficient of correlation deduced from a small sample, 1, 1921, pp. 3–32.
[46] S. Guo, C. Beleites, U. Neugebauer, S. Abalde-Cela, N.K. Afseth, F. Alsamad, S. Anand, C. Araujo-Andrade, S. Aškrabić, E. Avci, M. Baia, M. Baranska, E. Baria, L.A. Batista De Carvalho, P. De Bettignies, A. Bonifacio, F. Bonnier, E.M. Brauchle, H.J. Byrne, I. Chourpa, R. Cicchi, F. Cuisinier, M. Culha, M. Dahms, C. David, L. Duponchel, S. Duraipandian, S.F. El-Mashtoly, D.I. Ellis, G. Eppe, G. Falgayrac, O. Gamulin, B. Gardner, P. Gardner, K. Gerwert, E.J. Giamarellos-Bourboulis, S. Gizurarson, M. Gnyba, R. Goodacre, P. Grysan, O. Guntinas-Lichius, H. Helgadottir, V.M. Grošev, C. Kendall, R. Kiselev, M. Kölbach, C. Krafft, S. Krishnamoorthy, P. Kubryck, B. Lendl, P. Loza-Alvarez, F.M. Lyng, S. Machill, C. Malherbe, M. Marro, M.P.M. Marques, E. Matuszyk, C.F. Morasso, M. Moreau, H. Muhamadali, V. Mussi, I. Notingher, M.Z. Pacia, F.S. Pavone, G. Penel, D. Petersen, O. Piot, J.V. Rau, M. Richter, M.K. Rybarczyk, H. Salehi, K. Schenke-Layland, S. Schlücker, M. Schosserer, K. Schütze, V. Sergo, F. Sinjab, J. Smulko, G. D. Sockalingum, C. Stiebing, N. Stone, V. Untereiner, R. Vanna, K. Wieland, J. Popp, T. Bocklitz, Comparability of Raman spectroscopic configurations: a large scale cross-laboratory study, Anal. Chem. 92 (24) (2020) 15745–15756, https://doi.org/10.1021/acs.analchem.0c02696.
[47] K. Czamara, K. Majzner, M.Z. Pacia, K. Kochan, A. Kaczor, M. Baranska, Raman spectroscopy of lipids: a review, J. Raman Spectrosc. 46 (1) (2015) 4–20, https://doi.org/10.1002/jrs.4607.
[48] G. Socrates, Alkenes, oximes, imines, amidines, azo compounds: C=c, c=n, n=n groups, in: Infrared and Raman Characteristic Group Frequencies: Tables and Charts, third ed., John Wiley and Sons, 2004, p. 74.
[49] P. Hourant, V. Baeten, M.T. Morales, M. Meurens, R. Aparicio, Oil and fat classification by selected bands of near-infrared spectroscopy, Appl. Spectrosc. 54 (8) (2000) 1168–1174, https://doi.org/10.1366/0003702001950733.
[50] D. Cozzolino, I. Murray, A. Chree, J.R. Scaife, Multivariate determination of free fatty acids and moisture in fish oils by partial least-squares regression and near-infrared spectroscopy, LWT–Food Sci. Technol. 38 (8) (2005) 821–828, https://doi.org/10.1016/j.lwt.2004.10.007.
[51] ABB, Aocs standard procedure for iodine value (iv), Appl. Note 2 (2017).
[52] D.A. Nanton, A. Vegusdal, A.M.B. Rørå, B. Ruyter, G. Baeverfjord, B.E. Torstensen, Muscle lipid storage pattern, composition, and adipocyte distribution in different parts of atlantic salmon (salmo salar) fed fish oil and vegetable oil, Aquaculture 265 (1–4) (2007) 230–243, https://doi.org/10.1016/j.aquaculture.2006.03.053.
[53] P.V. Andersen, J.P. Wold, N.K. Afseth, Assessment of bulk composition of heterogeneous food matrices using Raman spectroscopy, Appl. Spectrosc. (2021), https://doi.org/10.1177/00037028211006150.
[54] J.E. Dessen, R. Weihe, B. Hatlen, M.S. Thomassen, K.A. Rørvik, Different growth performance, lipid deposition, and nutrient utilization in in-season (s1) atlantic salmon post-smolt fed isoenergetic diets differing in protein-to-lipid ratio, Aquaculture 473 (2017) 345–354, https://doi.org/10.1016/j.aquaculture.2017.02.006.
[55] T. Mørkøre, K.A. Rørvik, Seasonal variations in growth, feed utilisation and product quality of farmed atlantic salmon (salmo salar) transferred to seawater as 0 + smolts or 1 + smolts, Aquaculture 199 (1–2) (2001) 145–157, https://doi.org/10.1016/S0044-8486(01)00524-5.
[56] U. Nordgarden, B.E. Torstensen, L. Frøyland, T. Hansen, G.I. Hemre, Seasonally changing metabolism in atlantic salmon (salmo salar l.) ii - β-oxidation capacity and fatty acid composition in muscle tissues and plasma lipoproteins, Aquacult. Nutr. 9 (5) (2003) 295–303, https://doi.org/10.1046/j.1365-2095.2003.00260.x.
[57] F. Oppedal, A. Berg, R.E. Olsen, G.L. Taranger, T. Hansen, Photoperiod in seawater influence seasonal growth and chemical composition in autumn sea-transferred atlantic salmon (salmo salar l.) given two vaccines, Aquaculture 254 (1–4) (2006) 396–410, https://doi.org/10.1016/j.aquaculture.2005.10.026.
[58] B. Ruyter, C. Moya-Falcón, G. Rosenlund, A. Vegusdal, Fat content and morphology of liver and intestine of atlantic salmon (salmo salar): effects of temperature and dietary soybean oil, Aquaculture 252 (2–4) (2006) 441–452, https://doi.org/10.1016/j.aquaculture.2005.07.014.
[59] J.R. Sargent, D.R. Tocher, J.G. Bell, The lipids, in: J.E. Halver, R.W. Hardy (Eds.), Fish Nutrition, Academic Press, 2002.